

Considerations for Improving the Accuracy of Permittivity Measurement using Time Domain Reflectometry: Air-Water Calibration, Effects of Cable Length

D. A. Robinson,* M. Schaap, S. B. Jones, S. P. Friedman, and C. M. K. Gardner

ABSTRACT

In a paper presented by Heimovaara (1993) a method of calibrating TDR sensors was presented using air and water. Time has moved on but time domain reflectometry (TDR) sensors are still calibrated in a number of different ways. In this article we present a rigorous investigation of the method proposed by Heimovaara and demonstrate its accuracy. We demonstrate that the placement of a starting point in any place other than the one determined using Heimovaara's method results in erroneous permittivity measurement. This will be most significant at low values of permittivity. We propose that Heimovaara's method be adopted as a standard method for calibrating TDR sensors for measuring permittivity. The discussion centers on the placement of the first time marker used to measure the signal travel time from which permittivity is measured. Our modeling results suggest that this point is slightly forward of the apex of the bump on the waveform which corresponds to the impedance increase as the wave travels from the cable into the TDR sensor head. We also demonstrate that using the apex of this bump as a starting point reference can lead to erroneous measurements of travel time in layered dielectric media. Finally we examine the use of long cables to connect sensors to the TDR. We demonstrate that the travel time in the cable changes as a function of temperature and that fixed travel time markers based on cable length cause error in the measurement of travel time. For a 2.6-m cable the error was 1.6% at 50°C, and 4.7% for a 10.3-m cable, relative to calibration at 25°C. Software that tracks the sensor head either through the impedance mismatch caused by the head or using an electrical marker eliminates this source of error.

OBTAINING A permittivity measurement with TDR is relatively straightforward; to obtain good quality measurements with TDR requires careful TDR probe construction and waveform analysis. The measurement of porous media permittivity has been used to provide estimates of a number of physical properties including water content (Topp et al., 1980; Gardner et al., 2001; Noborio, 2001), porosity (Sen et al., 1981), surface area (Or and Wraith, 1999), and density (Perdok et al., 1996; Feng et al., 1999). The accuracy of these estimates depends on a two-stage calibration. The first element of this is the measurement of permittivity and the second is to obtain a calibration between permittivity and the estimated physical quantity. Time domain reflectometry has been proven to be a very successful technique for measuring the permittivity of materials. However, a number of methods and a variety of software packages with varying algorithms are used to analyze waveforms

to measure permittivity. In this discussion we will demonstrate the need for carefully choosing the correct waveform analysis method to obtain the best measurement of permittivity. This is crucial for the subsequent stage, which is the calibration between permittivity and the desired physical quantity. Errors in the measurement of permittivity are systematically carried over into the next calibration stage and can lead to erroneous interpretations of physical quantities.

The velocity (v) of an electromagnetic-plane wave propagating through a dielectric material is a function of both the relative permittivity (ϵ_r) and the relative magnetic permeability (μ_r) of the material.

$$v = \frac{c}{\sqrt{\mu_r \epsilon_r}} \quad [1]$$

The relative permeability in most soils (which are nonmagnetic) can be assumed equal to unity, making the velocity an inverse function of the square root of the permittivity. Conversely, the permittivity of a material can be calculated knowing the velocity of a wave travelling over a known distance in a transmission line. The permittivity measured using TDR is termed the apparent or measured permittivity (K_a), if the complete transmission line system is considered with back and forth wave propagation Eq. [2a] should be used and if only the one way travel time is considered as measured from the waveform Eq. [2b] is appropriate:

$$K_a = \left[\frac{ct_{s2}}{2L} \right]^2 \quad [2A]$$

$$K_a = \left[\frac{ct_{s1}}{L} \right]^2 \quad [2B]$$

where t_{s2} is the travel time in two directions and t_{s1} is the travel time in one direction only, usually in the range of nanoseconds, c is the velocity of light ($3 \times 10^8 \text{ m s}^{-1}$), and L is the length (m) of the probe over which the signal travels in a single direction. It is important to consider that this measured permittivity is a function of not only the energy storage of the dielectric material but also any losses that may arise because of ionic conductivity or dielectric relaxation phenomena. In many cases it is assumed that $K_a = \epsilon'$ where ϵ' is the real part of the permittivity associated with energy storage and dipole orientation. As White et al. (1994) demonstrated this is not always the case such that the measured permittivity of a material using a TDR transmission line is:

D.A. Robinson, and M. Schaap, George E. Brown Jr Salinity Laboratory USDA-ARS, 450 W. Big Springs Road, Riverside, CA 92507; S.B. Jones, Dep. Plants, Soils and Biometeorology, Ag. Sci Building-Old Main Hill 4820, Utah State University, Logan, UT 84322S; P. Friedman, The Institute of Soil, Water and Environmental Science, (ARO) The Volcani Center, Bet Dagan, Israel; and C.M.K. Gardner, Jesus College, University of Oxford, Oxford OX1 3DW, UK. Received 22 Jan. 2002. *Corresponding author (drobinson@ussl.ars.usda.gov).

$$K_a = \epsilon' \left[\left(1 + \sqrt{1 + \left(\frac{\epsilon''}{\epsilon'} \right)^2} \right) / 2 \right] \quad [3]$$

The imaginary part (ϵ'') is composed of relaxation losses, $\epsilon''_{\text{relaxation}}$ and ionic conductivity, σ_{dc} :

$$\epsilon'' = \epsilon''_{\text{relaxation}} + \frac{\sigma_{\text{dc}}}{2\pi f \epsilon_0} \quad [4]$$

Where, f is the frequency (Hz) and ϵ_0 is the permittivity in a vacuum (8.85 pF m^{-1}). Importantly, an increase in the imaginary component leads to increased TDR travel times and so higher measured permittivity values. In the work presented in this study the materials measured have negligible ionic conductivity and relaxation frequencies that do not interfere with the permittivity measurement in the TDR bandwidth so that the measured permittivity can be considered equivalent to the real part of the relative permittivity, discussed below.

In this introduction two sets of nomenclature are used; the symbol K is reserved for a measured feature using the TDR or any other instrument. The symbol ϵ is reserved for the permittivity of a material and is an intrinsic property of that material. When the material exhibits no losses $K_a = \epsilon'$, for most coarse sandy soils, which are none saline, this is true.

Calibration and Waveform Analysis for Permittivity Measurement

As demonstrated in Eq. [2b] the apparent permittivity is measured using the travel time (t_s) of the signal in a single direction along the length (L) of the TDR probe. Hence one needs to be able to find the point at which the wave leaves the sensor head and enters the probe electrodes and the point at which the signal is reflected. This can be demonstrated in a simple manner by placing a shorting bar across the electrodes. Figure 1 demonstrates three waveforms, one in air and then two with the probe shorted at the base of the electrodes (A) and at the tip of the electrodes (B). This gives a good impression of where the beginning and end of the probe are and the time interval that should be used to determine the permittivity.

Heimovaara's 1993 Method of Probe Calibration in Air and Water

All probes require calibration for accurate measurement of permittivity. Heimovaara (1993) presented a method of obtaining accurate calibration of a sensor using air and water. The analysis software presented in Heimovaara and de Water (1993) has a start and end reflection analysis mode. The software locates the base of the bump created by the impedance mismatch between cable and sensor head by fitting tangents (Fig. 2.2). It then locates the second reflection from the end of the sensor, denoted 'end point' in Fig. 2.1. The time between these two points is denoted as t_p (Fig. 2.1). The travel time t_p is a combination of the travel time of the signal in the sensor head (t_o) and the sensor electrodes (t_s). Heimovaara (1993) suggested that by taking measurements in air and water with known values of per-

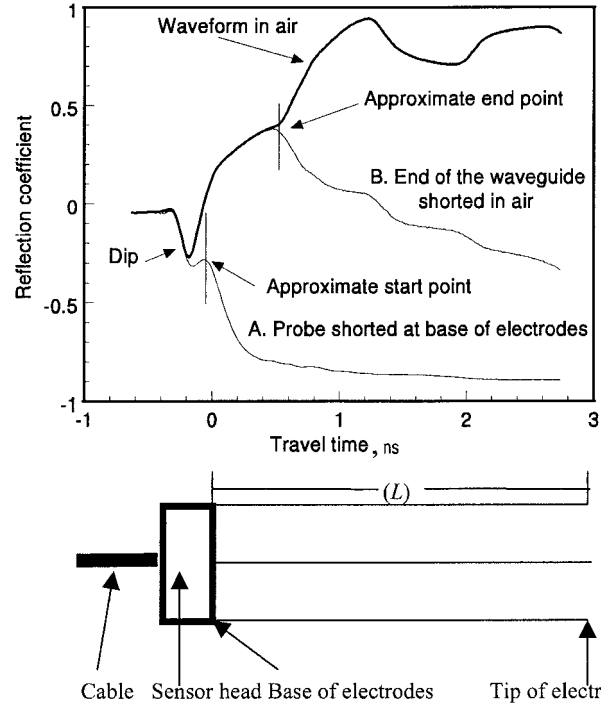


Fig. 1. Waveforms in air with a 20-cm probe shorted at (A) the base of the electrodes and (B) at the electrodes tips.

mittivity the travel time in the sensor itself (t_s) could be determined.

$$t_p = t_o + t_s = t_o + L \sqrt{\epsilon_r}/c \quad [5]$$

Where the symbols were defined for Eq. [2]. The above

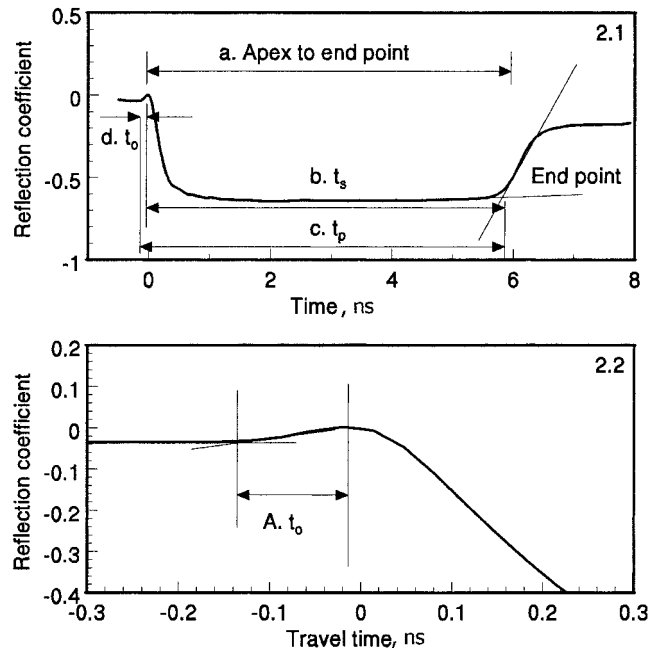


Fig. 2. (2.1) A waveform in water illustrating how the travel time is usually measured from the waveform. WINTDR measures from the apex of the bump to the end point located by the tangent lines. (2.2) The software of Heimovaara (1993) can either use a fixed start point based on cable length or can find the tangents for the first bump and calculate the travel time according to $t_s = t_p - t_o$.

equation can now be solved simultaneously for both water and air so that both L and t_0 can be found.

Alternative Methods of Measuring Travel Time

An alternative method to this procedure is to calibrate sensors using only water and to fix the starting reference at the apex of the bump as shown in Fig. 2.1. The travel time is then measured from the bump apex to where the tangent lines cross at the end of the waveform (t). Automated software such as WINTDR (Or et al., 1998) tracks the position of the bump apex locating the start point for travel time measurement at the apex (soilphysics.usu.edu). A similar method appears in Feng et al. (1999; Fig. 9) for the analysis software TDR++. Once the travel time is known, Eq. [2] is rearranged to solve for the probe electrical length (L). The value of L is often close to the physical length and the difference between this value and the physical length is considered to be because of a fringing electrical field at the end of the probe. The use of the apex of the peak is a somewhat arbitrary location for the start point of the probe chosen for the sake of convenience.

We will demonstrate the validity and accuracy of the method presented by Heimovaara (1993) and also show that at higher permittivity values negligible error is encountered using the bump apex as a starting reference point for measuring travel time. However, we will also demonstrate that the bump apex moves in layered material when a low permittivity region is above a high one. This is a commonly encountered phenomenon in coarse soils when there is a drying front.

Modeling of a TDR Transmission Line Using the Multisection Approach

The modeling of TDR waveforms has consistently been improved over the last decade. Yanuka et al. (1988) and Heimovaara (1994) presented a method of modeling the waveforms. Feng et al. (1999) presented a refined method that has similarities to the method of Yanuka et al. (1988). This model treats the transmission line with cable, sensor head, and electrodes as sections with differing impedance in a multisection transmission line. This method determines the frequency-domain scatter function of each section and subsequently computes the effective scatter function of the entire cable-sensor head-electrode system. A convolution of the input signal and scatter function followed by an inverse Fourier transform then leads to a time domain signal. For the details of the modeling, we refer the reader to the paper of Feng et al. (1999). This model was used to simulate waveforms for a system with a cable of 3 m having a permittivity of 2.295, equivalent to polyethylene, commonly used in cables. A 3-cm sensor head was used with permittivity of 1 but with three different impedances, 40, 50, and 60 ohms, achieved by altering the spacing ratio of the electrodes. Ten-centimeter electrodes were attached to this with impedance of 150 ohms in a vacuum. Waveforms with medium permittivities of 1, 5, 20, 40, 50, and 78.54 were generated with no relaxation. The input function used in the modeling was

obtained from a Tektronix TDR (1502C) (Tektronix, Beaverton, OR) with a perfect 50-ohm load attached to the cable tester, making the modeling more realistic.

Laboratory Experimentation

Instrumentation

Two types of TDR probes were used in our experimentation, a 20-cm coaxial probe with a 5-mm central conductor, 19.6 cm tall, in a 2.65-cm diameter outer cylinder, which was used for calibration measurements with dielectric fluids. The other probe used in the experimentation was a Soil Moisture Equipment Corp. 20-cm buriable probe (Soil Moisture Equipment Corp., Santa Barbara, CA). The probe has three stainless steel rods with a 6-mm central rod and two 3-mm outer rods at rod center spacing of 25 mm. An electrical marker (Dip in Fig. 1) is placed in the head of the sensor to ease the locating of the start point where the signal leaves the sensor head and enters the electrodes. The cable length was 1 m of Belden RG58 coaxial cable. The permittivity measurements were made with the probe attached to a Tektronix 1502C cable tester (Tektronix, Beaverton, OR) and the waveforms were collected with software developed by Heimovaara and de Water (1993).

Measurements

Three sets of experiments were performed; measurements in fluids using the coaxial cell, measurements in layers of water and air using the commercial sensor and an experiment using differing lengths of cable at different temperatures to determine the effect of cable length and temperature on the location of the apex of the first reflection.

Dielectric Fluids

Accurate measurements of permittivity (Lide, 1992) were made using air (1), penetrating oil (2.3), acetone (20.7), and water (78.5) at 25°C. The measurements were made in the coaxial cell previously described, in a constant temperature room at 25°C. The actual temperature of each of the fluids was measured before and after each set of ten measurements. Each of the liquids was chosen because of its negligible relaxation in the TDR frequency bandwidth, ensuring clear waveforms.

Measurements in Water–Air layers

The second experiment sequentially removed the three-wire probe, 1 cm at a time out of a cylinder of deionized water. The dimensions of the water column were 14.3 cm in diameter and 34.0 cm deep. The measurements were performed in a temperature-controlled laboratory at 25°C. The probe was calibrated using Heimovaara's above mentioned air-water calibration method.

Measurements Using Different Cable Lengths at Different Temperatures

The permittivity of a water-filled coaxial cell was measured using two different cable lengths of 2.6 and 10.3

m. The cables were placed in a circulating water bath that was used to control the temperature of both the coaxial cell with dimensions as previously described and attached cables; the temperature was varied from 1 to 50°C. Waveforms were analyzed for permittivity using WINTDR99 analysis software.

RESULTS AND DISCUSSION

Waveform Modeling

Modeled waveforms are presented in Fig. 3. The first diagram (0–2 ns) shows the input function obtained from the TDR. The line on the graph marked start of the input function is the location of the start of the input according to the fitting of a tangent line to the rising input signal (1.18 ns). From this point the amplitude of the input function increases until it reaches a maximum value of 0. Hilhorst (1998) proposed an estimate of the frequency bandwidth of the TDR signal based on electronic filter theory (Bird, 1980). The rise time (τ) is defined as the time it takes for the step function to reach 0.66 of its value after a first reflection. We chose the start point and end point to be the point at which the signal had risen 1% (1.14 ns) to the point where it reaches 66% (1.23 ns). This gave a rise time of 0.09 ns. The maximum passable frequency is then calculated according to, $f_{\text{TDR}} = 1/(2\pi\tau)$, which for the TDR gives a bandwidth of 1.768 GHz. This is in good agreement with the value given by Tektronix (Appendix C, Tektronix metallic TDR's for cable testing) who give a maximum passable frequency of 1.75 GHz. Friel and Or (1999) demonstrated with the aid of a spectrum analyzer connected to a Tektronix TDR that above 1 GHz the signal is mostly noise. This means that although the bandwidth of the TDR is wide, most of the power is concentrated between 0.01 and 1 GHz, however, this

corresponds to the optimal frequency range for determining soil water content.

The right-hand side of Fig. 3 shows two waveforms calculated for permittivities of 50 and 78.5. Note that there is no bump at the beginning of the waveform as the sensor head impedance was matched to the cable at 50 ohms. Knowing the permittivity of the cable, the sensor head and the material in which the electrodes are immersed one can calculate the points along the transmission line corresponding to the input signal entering the sensor head, leaving the sensor head, and being reflected from the end of the probe. The travel time equals $(\text{section length}/c) \times \sqrt{\epsilon_r}$, where c is the speed of light and ϵ_r is the permittivity of the section. These points are all marked on the diagram with dashed lines. The diagram also shows the modeled reflections for the cable and the sensor head terminated in an open circuit. These open reflections correspond with the calculated end of the cable head and end of the sensor head as demonstrated by the dashed lines in the figure.

The upper diagram in Fig. 4 shows computed waveforms for permittivities of 1 and 50. The diagrams below show a magnified section (16.2–17.0 ns) concentrating on the sensor head. Graphs are presented for sensor heads with three differing impedances, 40, 50, and 60 ohms. Clearly it can now be seen that the 40-ohm head causes a dip, the 50-ohm head is matched to the cable and no reflection results off the head, and the 60-ohm head results in a bump. This is the bump commonly observed when an unmatched TDR probe is attached to the cable tester; most TDR probe heads have impedances higher than 50 ohms causing this initial bump or spike on the wave trace. It is the apex of this bump, which is commonly used as the reference point to set the start time. These diagrams also suggest that the start point that should be used for measuring the time when

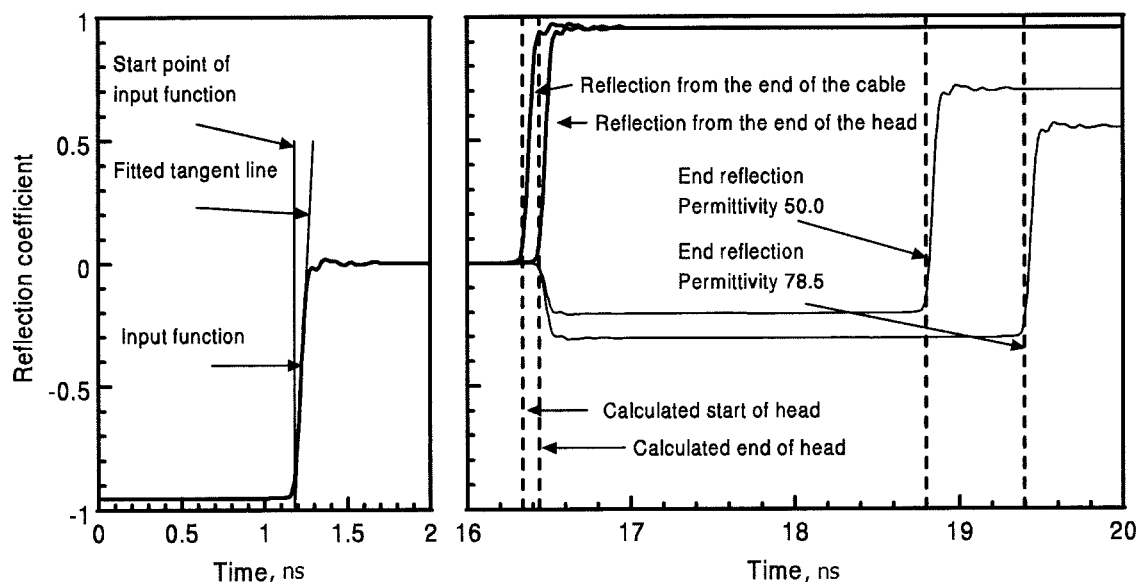


Fig. 3. The left-hand figure shows the input function with the point at which the first element of the signal leaves the cable tester. The right-hand diagram shows two waveforms for permittivities of 78.5 and 50. The dashed lines illustrate the calculated points at which the signal first enters the sensor head, leaves the sensor head and is reflected from the end of the probe respectively.

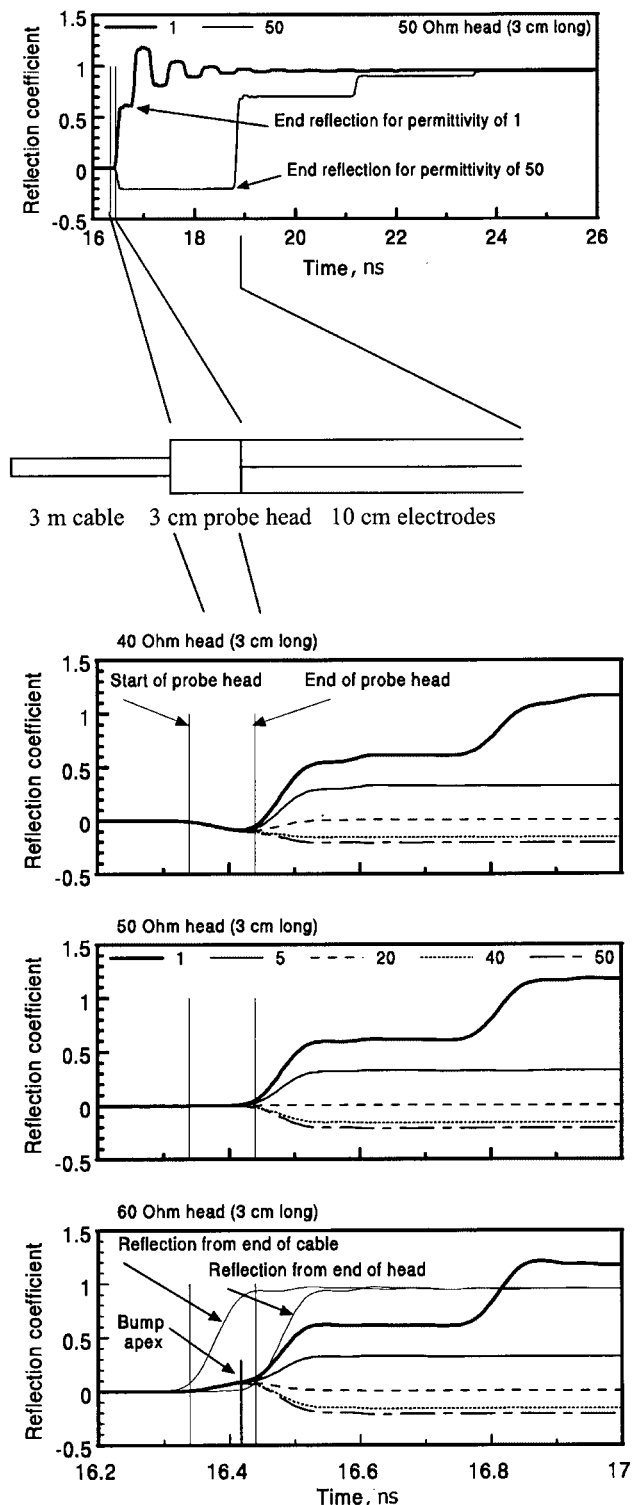


Fig. 4. The top figure shows modeled waveforms for permittivities of 1 and 50. The equivalent probe is shown below and then three graphs showing start points for sensors with 40, 50, and 60 ohm impedance heads, 3 cm long; the solid lines represent the calculated start and end of the sensor head. The 40-ohm head creates a dip in the waveform, the 50-ohm head is matched and the 60-ohm head creates a bump.

applying tangent fitting to the end reflection should be a little to the right of the apex of the bump. The amount will depend on the time width of the bump, which depends on the length of the sensor head and its permittivity. This is the same for all the heads but most clearly observed for the 60-ohm head (Fig. 4) where the bump apex is located at 16.42 ns and the calculated reflection from the end of the head is located at 16.44 ns. Measurements using a calibrated electrical length determined in water and using Eq. [2] can eliminate some of this error but it does mean that low permittivity values can be over estimated as we will go on to demonstrate using measurements.

Measurements in Dielectric Fluids

Measurements were made in four dielectric fluids that have negligible relaxation in the TDR frequency range. The waveforms are presented in Fig. 5 with approximate end reflection tangent line locations. The right-hand figure shows a close-up of the start of the waveforms as they enter the sensor electrodes. The apex points all fell in the same time location, forming a common reference point, the point being marked as the bump apex. This is important, as the start point does not depend on the medium permittivity for a homogeneous dielectric. We used the bump apex as measured in water as the reference point from which to measure t_p , to check the validity of Heimovaara's (1993) method. Using Eq. [5] and the travel time in water and air we calculated an electrical length of 0.1956 m and a value for t_0 of 0.035 ns. All travel times measured from the bump apex have the value of t_0 subtracted, the location of this point relative to the bump apex is indicated on Fig. 5 as the 'fixed start point'. Note that this is in agreement with the findings of the modeling that suggested it should lie to the right of the bump apex.

To demonstrate the effect of only calibrating in water and using start points other than the one described above the apex was set as the reference time marker. The travel time was then artificially increased and decreased by adding or subtracting increments of 0.02 ns from the reference time. This is equivalent to moving the start point to the left and right of the apex respectively (Fig. 6). The electrical length of the probe was then calculated for each measurement of time using only the travel time in water. The permittivity for the other three fluids was then calculated using their respective altered travel times with their corresponding electrical lengths determined from this calibration. The results are presented in Fig. 6 with permittivity as a log scale on the vertical axis. The horizontal lines show the actual permittivity values expected; the permittivity of water was fixed at 78.65 (24.7°C). The line marked with the arrow in the left-hand diagram is the calculated start point according to the method of Heimovaara and clearly demonstrates the validity of this permittivity calibration over the range of permittivity. The dashed line B marks the values that would have been obtained using only the peak apex as the reference and calibrating for the electrical length using only water. The other dashed

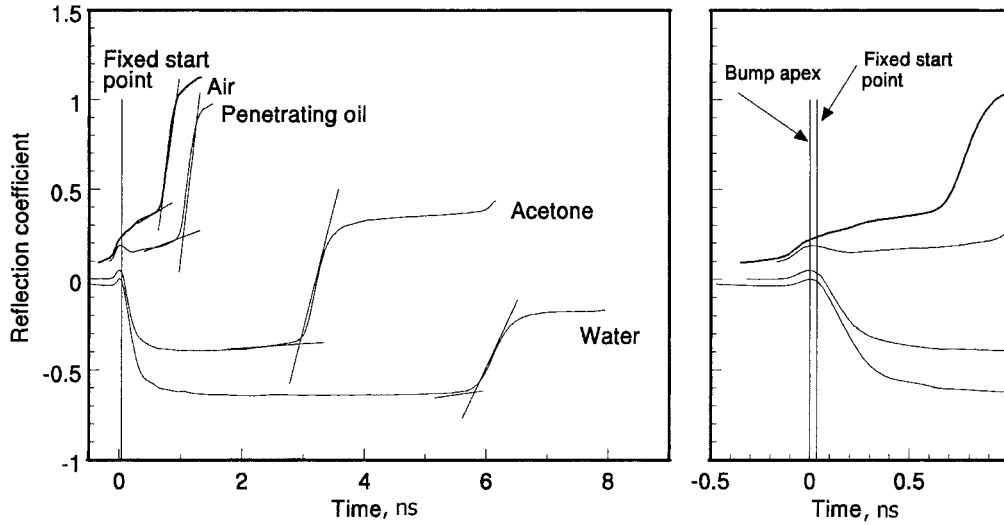


Fig. 5. Waveforms for water, acetone, penetrating oil, and air measured in a 19.5-cm coaxial cell. The right-hand figure illustrates the bump apex and the fixed start point that was found to correspond with cited permittivity values.

lines, A, C, and D clearly demonstrate that choosing an arbitrary start point and calibrating with only water produces increasingly erroneous results, especially at low permittivity values.

As expected from the waveform modeling, the required start point for accurate travel time measurement to obtain permittivity is slightly to the right of the bump apex, the amount will vary depending on the length of the sensor head. Interestingly, the value of the electrical length calculated by the method of Heimovaara was 0.1956 m, the physical length of the central electrode was measured as 0.196 m. This suggests that for a reasonably long coaxial cell the physical length and electrical length may be close in value. The practical implications of this analysis suggest that failing to position the marker according to the calibration method of Heimovaara (1993) will create an error in permittivity measurement that will increase toward small values of permittivity.

This potentially may result in overestimation of water content in dry soils but negligible errors in wet soils.

Measurements in Water–Air layers

The previous section demonstrated that to achieve accurate permittivity measurements a start point for travel time could be determined using a calibration in air and water. Calibration performed solely in water using the apex as the reference start point could introduce a small error at low permittivity values. However, using the apex as the start point for measuring travel time is convenient for software, which can easily locate this point. For monitoring applications calibration in water maybe sufficient for looking at changes in water content. However, in this section we go on to examine a specific case where using the apex can lead to enhanced erroneous permittivity determination at low permittiv-

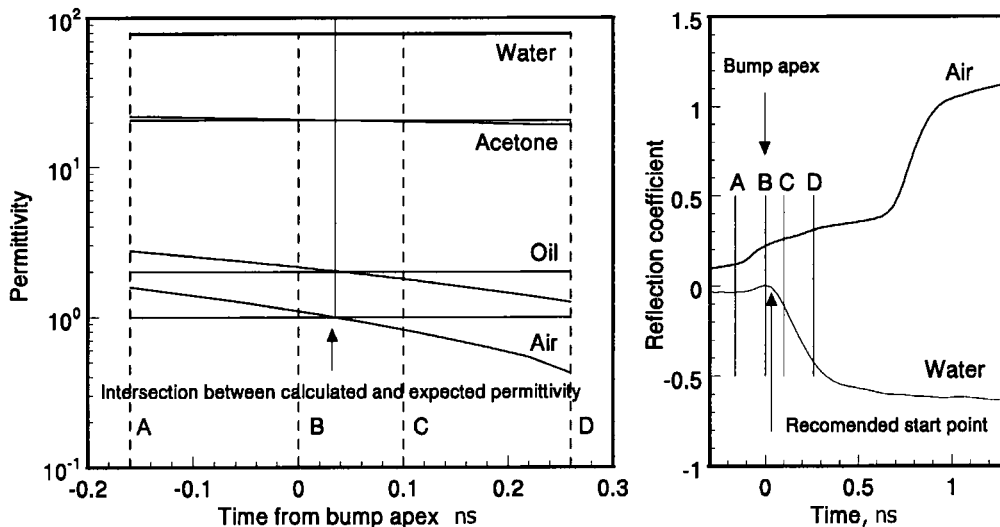


Fig. 6. Permittivity estimated from calibration of probe adjusting the electrical length of the probe according to measurements in water using the bump apex as a timing reference. The arrow on the left-hand diagram indicates to calibrated permittivity using Heimovaara’s calibration method. This point is located 0.035 ns to the right of the bump apex and corresponds to an electrical length of 0.1956 m. The dashed lines on the left-hand diagram correspond to the positions of the lines used to measure travel time on the right-hand diagram.

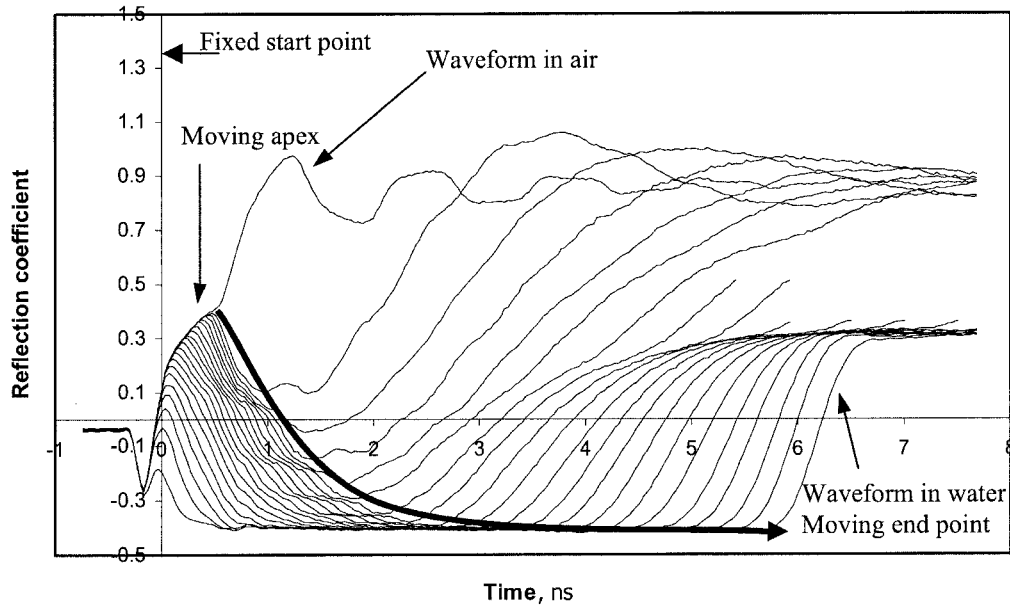


Fig. 7. A sequence of waveforms measured using a 20-cm probe sequentially dipped into a water column 1 cm at a time. Note how the bump apex at the start of the probe electrodes moves.

ity values. We examine the case of a probe inserted vertically downward into a low permittivity layer over a high permittivity layer, air–water in our case but layering of dry soil over moist soil commonly occurs, especially in coarse soils. Measurements were performed in layers of water and air. The waveforms collected with the probe sequentially dipped into water are presented in Fig. 7. The apex of the bump is observed to move forward in time as the probe is removed from the water.

Measurements made using vertically inserted TDR probes are often obtained from soils in which the soil surface is drying resulting in layering down the probe, this will be most distinct in sandy, coarse soils. The measured permittivity of layered dielectrics lends itself to theoretical analysis so that the expected apparent permittivity can be easily modeled. The propagation of an electromagnetic wave through a medium made up of alternating homogeneous dielectric layers has been previously analyzed (Birchack et al., 1974). The simplest way to analyze the problem is to refer to the time of travel through each layer, which is equal to:

$$t = \frac{f(L)}{v} = \frac{f(L)\sqrt{\epsilon}}{c} \quad [6]$$

where, f , is the volume fraction of a layer that is a function of its length (L), v , is the velocity of propagation through that layer, and c is the speed of light (3×10^8 m s^{-1}). The total time of propagation through for example a two-layer medium is therefore:

$$t_{\text{total}} = t_1 + t_2 = \sqrt{K_a} = f_1 \sqrt{\epsilon_1} + f_2 \sqrt{\epsilon_2} \quad [7]$$

The speed of light and the total lengths drop out of the equation. This equation has been expanded for three or more layers and is commonly termed the refractive index model. A note of caution must be added when using this model, which is it is only valid for thick layers compared with the traveling wavelengths. Chan and

Knight (2001) pointed out that as the ratio of wavelength to layer thickness increases above four the averaging regime changes from refractive index to arithmetic averaging of the permittivity, which they demonstrated using TDR. In the case of the layering used in our experiment the mean layer thickness was 10 cm and following Chan and Knight (2001) the effective frequency was about 750 MHz. This gives a wavelength varying according to $0.4/\sqrt{K_a}$, and values for wavelength over layer thickness of between 0.45 and 4, within the refractive index regime. For most purposes when TDR is used in soils with wet and dry layers the layers are of sufficient thickness to obey the refractive index regime.

A comparison of permittivity values using a stationary calibrated start point (0.0 ns, Fig. 7) and a start point moving with the bump apex are presented along with the refractive index model for air and water in Fig. 8. The point that we clearly demonstrate is that using the moving apex of the bump erroneously determines the permittivity, underestimating the value. The permittivity measurements made with the calibrated start point follow the refractive index model, which is the theoretical lower bound for the layered system, reasonably well. This has important consequences for measurements of water content. Errors carried forward to estimate water content from the determination of the permittivity, using the apex of the first reflection to determine permittivity, can create substantial underestimation if the prediction of water content is made using a standard calibration such as that of Topp et al. (1980). In addition to the error in the permittivity determination, one should take into account the large $d\theta/dK_a$ in the dry region of the permittivity water content calibration (Topp et al., 1980), making the relative error in water content greater than that of permittivity. An error of as much as 5 to 7% might be expected at the lower permittivity values.

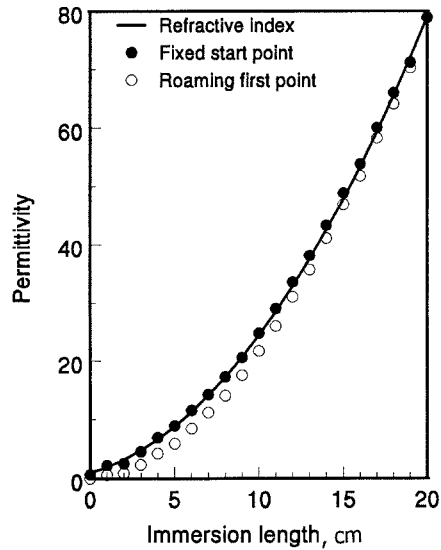


Fig. 8. Permittivity calculated as a function of immersion length using a fixed start point and one following the bump apex. Note how the moving apex causes underestimation of the permittivity.

Measurements Using Different Cable Lengths at Different Temperatures

Having determined a value for Δt_0 with Heimovaara's calibration method, it would be convenient to put a fixed value of cable length into the software, equivalent to the travel time in the cable. This is feasible and would reduce the analysis time if only one set of tangent lines has to be fitted to the waveform. This can be useful when large numbers of waveforms are to be analyzed. It is also especially useful in the particular case when the sensor head impedance matches the impedance of both the sensor head and soil so that no reflection occurs at the start of the waveform. This section demonstrates why this is not such a good idea in general, especially with longer cables and fluctuating temperatures.

In his paper on sensor design, Heimovaara (1993) pointed out that the use of long cables would seriously distort waveforms. Practically speaking, higher frequencies are filtered by the longer cable lengths and the waveforms become more rounded and harder to determine travel time from. Reece (1998) demonstrated that cable resistance affecting TDR measurement of electrical conductivity increases with cable length; however, this is not the issue here. In this final set of experiments we examine the issue of the effect of cable length on the position of the waveform as measured by the TDR. The changing temperature alters the permittivity of the dielectric in the cable and so changes the cable impedance. We found that the cable length between the TDR measurement device and the TDR probe held at different temperatures affects not only the magnitude of the bump but the position, effectively creating a time-shift of the bump as illustrated in Fig. 9. The start point bump of a TDR waveform, using a typical cable length of 2.6 m is compared with measurements using a 10.3-m cable for temperatures varying from 1 to 50°C. A leftward shift in the bump position corresponds to faster travel times in the coaxial cable resulting from higher

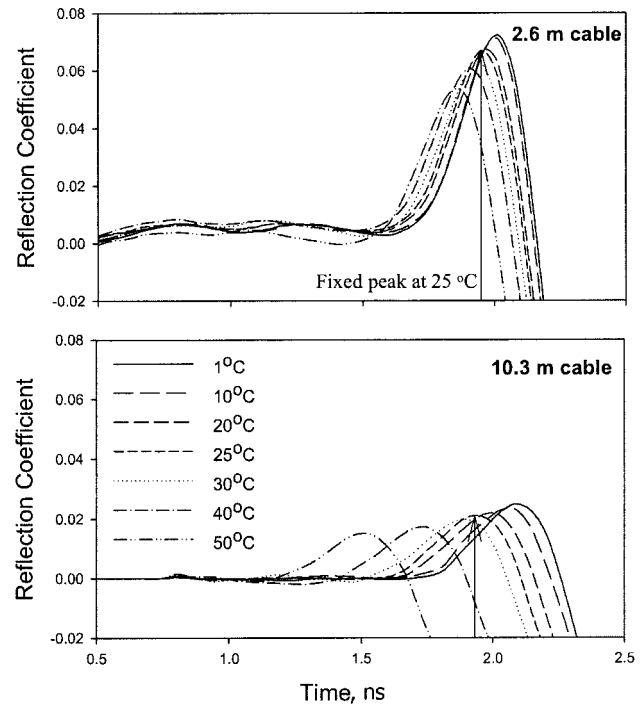


Fig. 9. Sensor-head waveform reflections for a probe and cable immersed in a constant temperature bath between 1 to 50°C. The upper figure is for a 2.6-m cable and the lower figure for a 10.3-m cable. Note how the reflection coefficient of the head reduces as the cable becomes longer and how it moves with temperature. Using a fixed start point in these circumstances would result in erroneous measurements.

temperatures. For measurements using a 'fixed' first reflection point, an error in the computed permittivity based on travel time analysis may result from cable temperature fluctuations, which are amplified by longer cable lengths. As an example of the type of error associated with using a 'fixed' time marker for the travel time start point, we calculated percentage error in water permittivities obtained from the waveforms shown in Fig. 9. Assuming a fixed first reflection point, the maximum error is associated with the greatest deviation from the fixed bump set at the calibration temperature (i.e., 25°C). For the 2.6-m cable the error was 1.6% at 50°C, (i.e., a measured permittivity of 69.0 instead of 70.1) and 4.7% for the 10.3-m cable (permittivity = 66.8). This highlights the importance of either working at a fixed temperature or using analysis software that hunts for the bump apex to locate the start point. Where the bump was tracked using analysis software, the measurement error was considerably less, being 0.8 and 1.1% for the 2.6- and 10.3-m cables, respectively. Automatic bump tracking features are available in WINTDR99 analysis software (Or et al., 1998), which allows a user-specified search window centered around the original bump, from which the waveform derivative is used to track the moving bump. It is also accommodated for in the software of Heimovaara and de Water (1993) when using their double reflection analysis.

As pointed out earlier the requirement for auto-tracking of the bump is the presence of an identifiable marker at the first reflection. As the modeling in Fig. 4

demonstrated when the head is matched to the cable at 50 ohms there is no bump. Soil Moisture Equipment Corps has developed a practical solution to this problem. They place an electrical marker in the head of the sensor so that no-matter what the length of the cable or impedance of the probe head a start point can always be easily located. The base of this dip can then be used as a reference for measuring Δt_p . An example of the dip caused by such an electrical marker can be seen in Fig. 1, marked 'Dip'. This greatly enhances the practicality of probes for field application with varying cable lengths at varying temperatures.

CONCLUSIONS

The method of Heimovaara, used for calibrating TDR probes using air and water is demonstrated to be accurate across the range of permittivity values. We would recommend that Heimovaara's method of calibration be adopted as the standard method for calibrating TDR sensors for permittivity measurements. Both modeling and measurements suggest that the location of the first time marker should be just to the right of the apex of the sensor head reflection on a TDR waveform. The use of the apex of the sensor head reflection will result in negligible errors in soil water content determination in relatively wet soil, but the errors will become more significant at low permittivity values. In addition to the error in the permittivity determination, one should take into account the large $d\theta/dK_a$ in the dry region of the permittivity-water content relationship, making the relative error in water content greater than that of permittivity. A number of practical issues regarding travel time analysis for permittivity measurement are then discussed. Measurements suggest that the apex of the sensor head reflection should not be used for measuring permittivity in strongly contrasting layered dielectric media. This is because the apex may move as the impedance of the sensor head and dry material may merge. We also demonstrate that the sensor head reflection moves according to the temperature of the cable; the amount increasing as the cable becomes longer. We suggest that a good practical solution to this problem for fieldwork is using probes with an electrical marker in the sensor head so that this acts as a reference from which travel time can be accurately measured.

ACKNOWLEDGMENTS

This research was supported in part by research grant No. IS-2839-97, from BARD, the United States-Israel Binational Agricultural Research and Development Fund. It was also supported in part by a USDA NRI grant (2002-3517-12S07).

REFERENCES

- Birchack, J.R., C.Z.G. Gardner, J.E. Hipp, and J.M. Victor. 1974. High dielectric constant microwave probes for sensing soil moisture. *Proc. IEEE* 62:93-98.
- Bird, G.J.A. 1980. Design of continuous and digital electronic systems. McGraw-Hill Book Co. Ltd, New York.
- Chan C.Y., and R. Knight. 2001. Laboratory measurements of electromagnetic wave velocity in layered sands. *Water Resour. Res.* 37:1099-1105.
- Feng W., C.P. Lin, R.J. Deschamps, and V.P. Drnevich. 1999. Theoretical model of a multisection time domain reflectometry measurement system. *Water Resour. Res.* 35:2321-2331.
- Friel R., and D. Or. 1999. Frequency analysis of time-domain reflectometry (TDR) with application to dielectric spectroscopy of soil constituents. *Geophysics* 64(3):1-12.
- Gardner, C.M.K., D.A. Robinson, K. Blyth, and J.D. Cooper. 2001. Soil water content. p. 1-64. *In* K.A. Smith and C.E. Mullins (ed.) *Soil and environmental analysis: Physical methods*. 2nd ed. Marcel Dekker, New York.
- Heimovaara, T.J. 1993. Design of triple-wire time domain reflectometry probes in practice and theory. *Soil Sci. Soc. Am. J.* 57:1410-1417.
- Heimovaara, T.J. 1994. Frequency domain analysis of time domain reflectometry waveforms 1. Measurement of the complex dielectric permittivity of soils. *Water Resour. Res.* 30:189-199.
- Heimovaara, T.J., and E. de Water. 1993. A computer controlled TDR system for measuring water content and bulk electrical conductivity of soils. Rep. 41. Laboratory of Physical Geography and Soil Science, University of Amsterdam, Amsterdam.
- Hilhorst, M.A. 1998. Dielectric characterisation of soil. PhD thesis, Wageningen. Publication Nr 98-01 DLO Institute of agricultural and environmental engineering (IMAG DLO), Wageningen, The Netherlands.
- Lide, D.R. 1992 *Handbook of chemistry and physics*. 73rd ed. CRC Press, London.
- Noborio, K. 2001. Measurement of soil water content and electrical conductivity by time domain reflectometry: A review. *Comput. Electron. Agric.* 31:213-237.
- Or, D., T. Hartwell, B. Fisher, R.A. Hubscher, and J.M. Wraith. 1998. WinTDR99—Users guide (windows-based time domain reflectometry program for measurement of soil water content and electrical conductivity). Utah Agric. Exp. Sta. Res. Rep., Logan, UT. [online] Available at <http://tal.agsci.usu.edu/%7Eetal/wintdr99/> (verified 1 Jan. 2002).
- Or, D., and J.M. Wraith. 1999. Temperature effects on soil bulk dielectric permittivity measured by time domain reflectometry: A physical model. *Water Resour. Res.* 35:371-383.
- Perdok, U.D., B. Kroesbergen, and M.A. Hilhorst. 1996. Influence of gravimetric water content and bulk density on the dielectric properties of soils. *Eur. J. Soil Sci.* 47:367-371.
- Reece, C.F. 1998. Simple method for determining cable length resistance in time domain reflectometry systems. *Soil Sci. Soc. Am. J.* 62:314-317.
- Sen, P.N., C. Scala, and M.H. Cohen. 1981. A self-similar model for sedimentary rocks with application to the dielectric constant of fused glass beads. *Geophysics* 46(5):781-795.
- Topp, G.C., J.L. Davies, and A.P. Annan. 1980. Electromagnetic determination of soil water content: Measurements in coaxial transmission lines. *Water Resour. Res.* 16:574-582.
- White, I., J.H. Knight, S.J. Zegelin, and G.C. Topp. 1994. Comments on "Considerations on the use of time domain reflectometry (TDR) for measuring soil water content". *Eur. J. Soil Sci.* 45:503-508.
- Yanuka, M., G.C. Topp, S. Zegelin, and W.D. Zebchuk. 1988. Multiple reflection and attenuation of time domain reflectometry pulses: Theoretical considerations for applications to soil and water. *Water Resour. Research*. 24:939-944.